Electrical Contact Resistance Theory for Conductive Rough Surfaces Separated by a Thin Insulating Film

L. Kogut and **K. Komvopoulos**

Department of Mechanical Engineering, University of California, Berkeley, California 94720

Abstract

An electrical contact resistance (ECR) theory is presented for conductive and rough (fractal) surfaces separated by a thin insulating film, which is treated as an energy barrier that impedes the current flow due to the electric-tunnel effect. The analysis yields insight into the effects of film properties, current flow, surface topography, mechanical properties, and contact load on the ECR. It is shown that the variation of the ECR with contact load is less pronounced than that observed in the absence of an insulating layer, due to the intrinsic voltage dependence of the tunnel resistance and the associated voltage compensation mechanism. The effect of the non-Ohmic behavior on the relations of the ECR with the contact load and the real contact area is discussed and results are compared with approximate analytical relations developed herein. The relation between the real contact area and the ECR depends on the current intensity and film properties and is independent of the surface topography and mechanical properties. Approaches for determining the surface roughness, mechanical properties, insulating film properties, and real contact area from ECR measurements are interpreted in light of the developed theory.

I. INTRODUCTION

Thin insulating films formed at the contact interfaces of components consisting of conductive materials play an important role in the performance of various electromechanical devices,[1-3] such as circuit breakers, connectors, relays, and switches. Significant advances in the development of reliable microrelays[4] and microswitches[5] that can be actuated electrostatically have been recorded recently. Although the contacting surfaces of these microdevices consist of structural polysilicon layers metallized with gold, there is a growing concern about the presence of contaminants and insulating films at contact interfaces that may greatly increase the ECR. For example, the formation of an insulating oxide layer on palladium, which is often used in small-size relays, has been reported to be the main cause for electrical contact deterioration.[6] Thus, there is a great demand for new materials that can increase the device lifetime, while maintaining a low and stable contact resistance for a long period.[7]

The high tunnel resistance due to an insulating thin film may degrade the performance of components produced with various bonding techniques, such as conductive adhesive joints,[8,9] flip-chip bonding and ball-grid array socket,[10] and resistance spot welding.[11] Moreover, the existence of native insulating oxides prevents the use of certain materials in joining applications.[12] Despite the fact that in most applications a low ECR is desirable for better performance,[13] there are also situations where a high ECR enhances the device lifetime.[14] The strong effect of an insulating film on the ECR is beneficial in many applications, such as hydrogen detection,[15] determination of the properties of surface oxides,[16] and detection of film formation at sliding interfaces.[17] Therefore, it is important to understand the role of a thin insulating film in ECR measurements.

One of the early ECR models that takes into account the presence of a thin film adsorbed at the surfaces is attributed to Holm,[18] who observed that the ECR is affected by both the constriction

resistance and the film resistance. A generalized ECR theory[19] that uses fractal geometry for surface topography description,[20] elastic-plastic deformation of the contacting asperities,[21] and size-dependent electrical constriction resistance of the microcontacts[22] comprising the real contact area was recently developed for homogenous conductive surfaces. In general, theoretical predictions for homogenous conductive surfaces underestimate the measured ECR in the presence of thin insulating films at the surfaces.[23] In a previous ECR study,[24] a surface thin film was modeled as an ideal insulating material. However, when two surfaces are separated by a sufficiently thin insulating film, it is possible for current to flow due to the tunnel effect.[25] A more recent ECR study that accounts for the presence of interfacial insulating thin layers[26] was based on the general theory of the electric-tunnel effect between similar electrodes separated by a thin insulating film.[27] An equivalent electric circuit for the contact interface was proposed[26] and the current intensity and voltage drop across the interface were found to be in good agreement with experimental results. However, although the equivalent electrical circuit proposed in Ref. 26 characterizes the global behavior at the contact interface, it does not account for the physical behavior of the microcontacts.

Another shortcoming of a previous ECR model[24] that was based on a detailed analysis at the asperity microcontact level is the use of a statistical approach to represent the surface topography.[28] This approach is limited by the dependence of statistical roughness parameters on the sampling length and the resolution of the measuring instrument and, therefore, cannot yield unbiased information about the surface topography, which plays an important role in the ECR measurements. This deficiency can be overcome by using a fractal topography description that is based on scale-invariant parameters.[29] Fractal geometry provides an effective means of modeling engineering surfaces exhibiting random, multi-scale topographies due to its intrinsic advantages of scale invariance and self-affinity.[30] A fractal contact analysis that accounts for the elastic, elastic-plastic, and fully plastic

deformation of the asperity microcontacts at rough surfaces with fractal topography description was derived in a recent study.[21]

Although the previous ECR studies have yielded valuable insight into the origins of the ECR, a general theory for conductive, elastic-plastic, and rough surfaces separated by a thin insulating film has not been developed yet. Thus, the main objective of this study was to produce a general ECR theory for conductive surfaces separated by a thin insulating film. The present ECR theory is based on fractal geometry for surface topography description,[20] elastic, elastic-plastic, and fully plastic deformation of the asperity microcontacts,[21] and quantum mechanics considerations for the electric-tunnel effect through the thin insulating film.[27] It is demonstrated that the constriction resistance is negligible with respect to the tunnel resistance. This means that the ECR behavior can be profoundly changed in the presence of an insulating thin film at the contact interface. Consequently, there is a marked difference with the theory derived for conductive rough surfaces,[19] where the constriction resistance is the only mechanism that impairs the current flow.

II. THEORETICAL TREATMENT

A. Surface description

Fractal geometry[30] provides a means of overcoming limitations associated with the resolution of the instrument used to measure surface roughness parameters. Two important parameters in fractal topography description are the fractal roughness G and the fractal dimension D ($2 < D < 3$). The fractal roughness G is a height scaling parameter independent of frequency. A rougher surface is characterized by higher G values. The fractal dimension D determines the contribution of high- and low-frequency components in the surface profile. Hence, high values of D indicate that high-frequency components are more dominant in the surface profile than low-frequency components. For fixed fractal roughness G, higher values of the fractal dimension D yield smoother topographies;

however, the amplitude ratio of high-to-low frequencies of the surface increases with *D*. Details about the characterization of the surface topography using fractal geometry can be found elsewhere[19-21,29-31] and, therefore, are not repeated here for brevity.

B. Mechanical contact model

Contact of two rough surfaces [Fig. 1(a)] is equivalent to the contact of a smooth (flat) half-space with reduced elastic modulus $E = \left[\left(1-\nu_1^2\right)/E_1 + \left(1-\nu_2^2\right)/E_2\right]^{-1}$**, where** ν_1**,** ν_2**, and** E_1**,** E_2 **are the Poisson's ratios and elastic moduli of the two surfaces, respectively, and a rigid rough surface with topography equivalent to those of the two rough surfaces[32] [Fig. 1(b)]. For fractal surfaces, this implies that the power spectrum of the equivalent rough surface is equal to the sum of the power spectra of the two surfaces [Fig. 1(b)].[31] The equivalent thickness *t* of an insulating film covering the surfaces is $t = t_1 + t_2$, where t_1 and t_2 denote the thickness of the film on each surface. For very thin films (i.e., $t <$ 50 Å),[16] where the electric-tunnel effect occurs, the contact mechanics of layered media is dominated by the mechanical properties of the substrate.[21] Surface contact produces numerous circular asperity microcontacts [Fig. 1(b)], assumed to be sufficiently apart from each other in order for asperity interactions to be secondary. This assumption is reasonable for lightly loaded contacts where the real contact area *A* is a small fraction of the apparent contact area A_a.[28] Based on these assumptions and the calculated mean contact pressure and contact area of the asperity microcontacts, the total contact load *P* and real contact area can be obtained using an integration procedure that accounts for the microcontact contributions to the previous contact parameters.[20,21]**

For the case of fully plastic deformation of all the microcontacts, an explicit relation between the real contact area and the contact load can be obtained because the mean contact pressure is equal

to the hardness of the softer surface H, assumed equal to cY, where Y is the yield strength and c is typically equal to 2.8.[33] Hence, the following relation that is independent of surface topography is obtained[34]

$$A^* = (E/H)P^*, \tag{1}$$

where the dimensionless real contact area and contact load are defined as $A^*=A/A_a$ and $P^*=P/(A_aE)$, respectively.

For the cases of elastic or fully plastic microcontact deformation, the total contact load and real contact area, determined analytically by integrating the contribution of the elastic and fully plastic microcontacts, are given by[19]

$$P^* = \frac{cY}{E}\left(\frac{D-1}{3-D}\right)a_L'^*\left[\left(\frac{a_c'^*}{a_L'^*}\right)^{(3-D)/2} - \left(\frac{a_S'^*}{a_L'^*}\right)^{(3-D)/2}\right] + \\ + \frac{2^{(11-2D)/2}}{3\pi^{(4-D)/2}}\left(\frac{D-1}{5-2D}\right)(\ln\gamma)^{1/2}G^{*(D-2)}(a_L'^*)^{(4-D)/2}\left[1-\left(\frac{a_c'^*}{a_L'^*}\right)^{(5-2D)/2}\right] \tag{2}$$

and

$$A^* = \frac{D-1}{2(3-D)}a_L'^*\left[\left(\frac{a_c'^*}{a_L'^*}\right)^{(3-D)/2} - 2\left(\frac{a_S'^*}{a_L'^*}\right)^{(3-D)/2} + 1\right]. \tag{3}$$

The dimensionless fractal roughness G^* is defined as $G^* = G/A_a^{1/2}$, γ is a scaling parameter used in the fractal description of the surface topography (typically, γ = 1.5),[20] and a_S' and a_L' are the smallest and largest truncated microcontact areas, respectively.[21] The critical truncated microcontact area a_c' separating the elastic from the fully plastic deformation regime is given by[19,20]

$$a_c' = \left[2^{(9-2D)}\pi^{(D-2)}b^{-1}G^{(2D-4)}\left(\frac{E}{cY}\right)^2\ln\gamma\right]^{1/(D-2)}, \tag{4}$$

where $b = [\pi(0.454 + 0.41\nu_1)/2]^2$, in which ν_1 is the Poisson's ratio of the softer material. Microcontacts with truncated contact areas $a' > a_c'$ and $a' \le a_c'$ are in the elastic and fully plastic deformation regimes, respectively.[20] The above microcontact areas are normalized with respect to A_a and the dimensionless parameters are denoted by an asterisk.

Relations for the mean contact pressure and contact area have been derived for a single asperity in the elastic, elastic-plastic, and fully plastic deformation regimes.[21] However, because the constitutive relations for elastic-plastic deformation are more complex than those of the simpler elastic and fully plastic deformation,[20] a numerical integration scheme was developed in order to calculate the total contact load and real contact area.[21] Consequently, the total contact load and real contact area can be obtained as

$$P = \sum_{i=1}^{N(a_S')} F_i \qquad \textbf{(5)}$$

and

$$A = \sum_{i=1}^{N(a_S')} a_i \textbf{ ,} \qquad \textbf{(6)}$$

where $N(a_S')$ is the number of truncated asperities possessing areas greater than the smallest truncated contact area a_S'. The contact load F_i and contact area a_i of the ith microcontact are calculated using the appropriate constitutive relations.[21]

C. Electrical contact resistance at a single microcontact

The ECR at each microcontact R_i consists of the constriction resistance R_{ci} due to the convergence and divergence of current flow[18] and the tunnel resistance R_{ti} due to the presence of an insulating film introducing a potential barrier that impedes the flow of electrons.[27] An electrical analog of the total contact resistance due to the constriction resistance produced by the microcontacts

comprising the real contact area and the insulating film between the contacting surfaces is presented in Fig. 1(c). It has been shown[19] that for lightly loaded surfaces, where the radius of each microcontact r_i is smaller than the average electron mean-free path of the contacting surfaces, $\lambda = (\lambda_1 + \lambda_2)/2$, the constriction resistance is dominated by the Sharvin mechanism. According to this mechanism, the electrons travel through the microcontacts without undergoing any scattering, and the constriction resistance is given by[35]

$$R_{ci} = \frac{\lambda \rho}{a_i}, \tag{7}$$

where ρ is the average specific resistivity of the contacting surfaces, $\rho = (\rho_1 + \rho_2)/2$.

For electrons to pass from one surface to the other in the presence of an insulating film they must have sufficient energy to surmount the barrier produced by the insulating film, i.e., they must enter the conduction band of the insulator, a process known as thermionic emission. According to classical physics, the electrons cannot penetrate through the barrier if the electron energy is less than the height of the interfacial barrier. However, according to quantum theory, a finite probability exists for the electrons to tunnel through the barrier, depending on the size and shape of the barrier encountered by the electrons.

Simmons[27] developed a formula for electric tunneling through a potential barrier of an arbitrary shape, existing in a thin insulating film that separates two similar electrodes. The formula was derived for a rectangular barrier including the image force. The effect of the image force is to reduce the area of the potential barrier by rounding off the corners of its distribution, thereby reducing the thickness of the barrier and, consequently, increase the current flow between the electrodes. The analysis presented in Ref. 27 is for low temperatures, where the thermal current can be neglected, thus restricting the electron transport between electrodes to the tunnel effect. However, it has been shown[16] that the equations derived in Ref. 27 are also applicable at higher temperatures.

Consider a single microcontact of area a_i [Fig. 1(b)] covered by a thin insulating film of thickness t, dielectric constant K, and energy height above the Fermi level of the conductive surfaces φ_o. The current intensity I_i through the microcontact and associated voltage drop V_i in three different voltage regimes are given by[27]

$$I_i = \left(3.16\times10^{10}/\Delta S\right)\varphi_L^{1/2}\exp\left(-1.025\Delta S\varphi_L^{1/2}\right)V_i a_i, \qquad \text{for } V_i \cong 0 \tag{8}$$

where

$$\varphi_L = \varphi_0 - \left[5.75/\left(K\Delta S\right)\right]\ln\left[\frac{S_2\left(t-S_1\right)}{S_1\left(t-S_2\right)}\right], \tag{9}$$

and

$$\Delta S = S_2 - S_1, \tag{10a}$$

where S_1 and S_2 are given by

$$S_1 = 6/\left(K\varphi_0\right), \tag{10b}$$

and

$$S_2 = t - 6/\left(K\varphi_0\right). \tag{10c}$$

The tunnel resistance R_{ti} for $V_i \cong 0$ is derived from Eq. (8) as

$$R_{ti} = \frac{V_i}{I_i} = \frac{\Delta S\exp\left(1.025\Delta S\varphi_L^{1/2}\right)}{3.16\times10^{10}\varphi_L^{1/2}}\frac{1}{a_i}. \tag{11}$$

Equation (11) shows that R_{ti} is independent of the voltage or the current applied to the microcontact to measure the tunnel resistance and, therefore, is an Ohmic resistance. As can be seen from Eqs. (9) – (11), R_{ti} is inversely proportional to a_i and increases with t, K, and φ_0.[27]

For a voltage drop across a microcontact V_i that is not very small,[27]

$$I_i = \left[6.2\times10^{10}/\left(\Delta S\right)^2\right]\left\{\varphi_L\exp\left(-1.025\Delta S\varphi_L^{1/2}\right) - \left(\varphi_L + V_i\right)\exp\left[-1.025\Delta S\left(\varphi_L + V_i\right)^{1/2}\right]\right\}a_i, \tag{12}$$

where

$$\varphi_L = \varphi_0 - [V_i/(2t)](S_1 + S_2) - [5.75/(K\Delta S)]\ln\left[\frac{S_2(t-S_1)}{S_1(t-S_2)}\right], \tag{13}$$

and

$$S_1 = 6/(K\varphi_0), \tag{14}$$

$$S_2 = t[1 - 46/(3\varphi_0 Kt + 20 - 2V_i Kt)] + 6/(K\varphi_0), \qquad \text{for } V_i < \varphi_0 \tag{15a}$$

or

$$S_2 = (\varphi_0 Kt - 28)/KV_i, \qquad \text{for } V_i > \varphi_0. \tag{15b}$$

As can be seen from Eq. (12) the relation between current and voltage is nonlinear. Therefore, it is not possible to derive an explicit relation for the tunnel resistance, such as that given by Eq. (11). Moreover, because φ_L and ΔS are functions of the voltage, the tunnel resistance is non-Ohmic and decreases with increasing voltage.[27]

In Eqs. (8) – (15), and throughout this study, I_i is expressed in A, V_i and φ_0 in V, t, S_1, and S_2 in Å, and a_i (as well as all other areas) in cm^2.

III. APROXIMATE ANALYSIS

To obtain insight into the contact electromechanics behavior, it is instructive to first consider the following analysis derived for the low-voltage regime ($V_i \cong 0$) and either elastic and fully plastic microcontacts or solely fully plastic microcontacts. Figure 1(c) shows that the constriction resistance and the tunnel resistance of a microcontact are in series. The ratio between the restriction resistance and the tunnel resistance in the low-voltage regime ($V_i \cong 0$) is obtained by dividing Eq. (7) by Eq. (11)

$$\frac{R_{ci}}{R_{ti}} = \frac{3.16\times10^{10}\varphi_L^{1/2}\lambda\rho}{\Delta S\exp(1.025\Delta S\varphi_L^{1/2})}. \tag{16}$$

When $R_{ci}/R_{ti} << 1$, the constriction resistance can be neglected in favor of the tunnel resistance. The ratio R_{ci}/R_{ti} is examined for a conductive surface possessing a fairly high resistivity of $\rho = 10^{-4}\ \Omega\,\text{cm}$ and $\lambda = 3\times10^{-6}$ cm, and a relatively low energy barrier with $t = 10\,\text{Å}$, $\varphi_0 = 1$ V, and $K = 4$. For this case, Eqs. (9), (10), and (16) yield $R_{ci}/R_{ti} = 2.7\times10^{-3}$, indicating that the constriction resistance can indeed be neglected as secondary; hence, the contact resistance at a microcontact is $R_i \cong R_{ti}$. This is a reasonable approximation for conductive surfaces separated by a thin insulating film, especially if the surfaces are very conductive and the energy barrier imposed by the insulating film is higher and/or wider. Equation (16) is valid when $V_i \cong 0$, i.e., when the tunnel resistance is Ohmic. For higher voltages, the tunnel resistance [Eqs. (12) – (15)] decreases with increasing voltage drop[27] and, hence, the ratio R_{ci}/R_{ti} increases. As shown in Ref. 27, the tunnel resistance decreases by approximately an order of magnitude when the voltage increases from 0 to 1 V. However, despite this effect, the ratio R_{ci}/R_{ti} assumes values significantly less than one.

As mentioned in Sec. IIB, the equivalent contact model of two rough surfaces consists of a smooth elastic-plastic medium in contact with a rigid rough surface. The corresponding real contact area is the summation of the discrete asperity microcontacts. The total ECR is assumed to be the sum of individual parallel resistances corresponding to the restriction resistances of individual microcontacts.

The electrical conductivity C_i of a single microcontact in the low-voltage regime ($V_i \cong 0$) is obtained from Eq. (11) as

$$C_i = R_i^{-1} = \frac{3.16\times10^{10}\,\varphi_L^{1/2}\exp\left(-1.025\Delta S\varphi_L^{1/2}\right)a_i}{\Delta S}. \tag{17}$$

Using an integration procedure for elastic and fully plastic microcontacts,[19] the total electrical conductivity C is obtained as

$$C = \int_{a_S'}^{a_c'} C_{ip}(a')n(a')da' + \int_{a_c'}^{a_L'} C_{ie}(a')n(a')da', \quad \textbf{(18)}$$

where $n(a')$ is the size distribution function of truncated microcontacts,[20] and the subscripts p and e denote plastic and elastic, respectively. The electrical conductivity of a single microcontact in the elastic and fully plastic deformation regimes, C_{ie} and C_{ip}, respectively, can be obtained by substituting the appropriate contact area relations[20] into Eq. (17). After integration, Eq. (18) yields

$$C = \frac{3.16\times10^{10}\varphi_L^{1/2}\exp\left(-1.025\Delta S\varphi_L^{1/2}\right)}{\Delta S}\frac{D-1}{2(3-D)}a_L'\left[\left(\frac{a_c'}{a_L'}\right)^{(3-D)/2} - 2\left(\frac{a_S'}{a_L'}\right)^{(3-D)/2} + 1\right]. \quad \textbf{(19)}$$

The dimensionless electrical conductivity C^* is defined as

$$C^* = \frac{Ct}{3.16\times10^{10}\varphi_0^{1/2}A_a} = \left(\frac{\varphi_L}{\varphi_0}\right)^{1/2}\left(\frac{t}{\Delta S}\right)\exp\left(-1.025\Delta S\varphi_L^{1/2}\right)\frac{D-1}{2(3-D)}a_L'^*\left[\left(\frac{a_c'^*}{a_L'^*}\right)^{(3-D)/2} - 2\left(\frac{a_S'^*}{a_L'^*}\right)^{(3-D)/2} + 1\right] \quad \textbf{(20)}$$

and, thus, the dimensionless ECR can be expressed as

$$R^* = \left(C^*\right)^{-1} = \frac{3.16\times10^{10}\varphi_0^{1/2}A_a}{t}R. \quad (21)$$

From Eqs. (4), (9), (10), (20), and (21) it can be seen that the dimensionless ECR depends on the fractal parameters D and G^*, the mechanical properties E/Y and ν_1, the insulating film thickness t and properties K and φ_0, and the dimensionless smallest and largest truncated microcontact areas $a_S'^*$ and $a_L'^*$, respectively. For a continuum description, a_S' must be greater than the atomic dimensions, e.g., about six times the lattice dimension.[21] For given surface roughness, mechanical properties, and insulating film properties, the only unknown parameter in Eq. (20) is $a_L'^*$, which can be found implicitly from Eq. (2) as a function of the contact load P^*. Substitution of the obtained value of $a_L'^*$ into Eq. (3) yields the corresponding real contact area A^*. Alternatively, the value of

$a_L'^*$ obtained from ECR measurements and Eq. (20) can be substituted into Eq. (2) to estimate the corresponding contact load and, in turn, the adhesion force and adhesion energy. This approach was adopted in a recent theoretical treatment of adhesion of homogenous conductive surfaces.[34] Because the determination of the real contact area as a function of contact load using Eqs. (2) and (3) involves the surface topography parameters D and G^*, the analysis is applicable for static contact conditions. Estimation of the real contact area using the previous approach in the case of dynamic contacts can be accomplished by using the fractal parameters of the evolved (current) surface topography. This applies also to the alternative approach used to obtain the contact load as a function of the ECR from Eqs. (2), (20), and (21).

Dividing Eq. (3) by Eq. (20) yields

$$A^* = \left(\frac{\varphi_0}{\varphi_L}\right)^{1/2} \left(\frac{\Delta S}{t}\right) \exp\left(1.025 \Delta S \varphi_L^{1/2}\right) \left(R^*\right)^{-1}. \tag{22}$$

In view of Eq. (22), the real contact area can be directly obtained from simple ECR measurements that are independent of the surface topography and mechanical properties of the contacting surfaces and the applied load, provided the voltage drop is very small. The relation between the real contact area and the ECR in the low-voltage regime [Eq. (22)] reveals a dependence only on the properties of the thin insulating film. This is expected due to the dependence of the ECR on the microcontact area and film properties [Eq. (11)]. Although Eq. (22) was derived for either elastic or fully plastic microcontacts, it is applicable to the entire deformation range because of the intrinsic relation between the contact area and the ECR existing at the single asperity level [Eq. (11)].

For the simple case of fully plastic microcontacts, an explicit relation between the ECR and the contact load that is independent of surface topography can be obtained for the low-voltage regime by using Eqs. (1) and (22),

$$P^* = \frac{H}{E}\left(\frac{\varphi_0}{\varphi_L}\right)^{1/2}\left(\frac{\Delta S}{t}\right)\exp\left(1.025\Delta S\varphi_L^{1/2}\right)\left(R^*\right)^{-1}. \quad (23)$$

Equation (23) can be used to determine the adhesion energy and adhesion force in dynamic contacts, where the surface topography may change during operation due to deformation of the asperity microcontacts, similar to the method proposed for homogenous conductive surfaces.[34]

IV. NUMERICAL ANALYSIS

To obtain a general theory, it is necessary to account for the elastic-plastic deformation of the asperity microcontacts[21] and the voltage-dependence of the tunnel resistance [(Eqs. (12), (13), and (15)].[27] However, the complex constitutive relations of the contact parameters in the elastic-plastic deformation regime and the non-Ohmic behavior of the tunnel resistance [Eqs. (12) – (15)], i.e., the dependence of the tunnel resistance of a microcontact on the voltage drop, inhibit the derivation of closed form solutions. Therefore, a numerical scheme[21] was used to obtain results for the various contact parameters. The previous numerical scheme was updated in the present study to include an iterative procedure for the tunnel resistance. The procedure involves assuming an initial value of the voltage drop V across the contact interface [Fig. 1(c)] and because all the microcontacts are connected in parallel and R_{ci} is negligible compared to R_{ti}, this is also the value of the voltage drop V_i across each microcontact due to the tunnel effect. The current I_i that flows through each microcontact is then calculated according to the appropriate voltage range [i.e., Eq. (8) or Eq. (12)]. Then, the total contact load and real contact area are obtained using Eqs. (5) and (6), respectively, and the total current I is calculated by

$$I = \sum_{i=1}^{N(a_S')} I_i \,, \quad \textbf{(24)}$$

Subsequently, the calculated total current is compared with the applied current and the assumed value of the voltage drop is adjusted accordingly. This procedure is repeated until the variation of the

total current converges to a specified small tolerance value (e.g., 1%). Then, the total ECR is determined from the definition of the electrical resistance $R = V / I$.

V. RESULTS AND DISCUSSION

In this section, numerical results are presented for three-dimensional surfaces, generated using fractal geometry for $A_a = 1$ m^2, $2 < D < 2.5$,[36] $10^{-17}\,\text{m} \le G \le 10^{-13}\,\text{m}$ (i.e., $10^{-11} \le G^* \le 10^{-7}$), $a_S' = 1$ nm^2, and $10^{-4} \le A^* \le 10^{-2}$, separated by a thin insulating film. The upper and lower limits of A^* are selected to yield a small average size of microcontacts relative to their average spacing in order for interaction effects to be secondary and extremely small real contact areas with unrealistically small number of asperity microcontacts do not occur. Thus, the curves shown in the following figures are bounded by the contact loads corresponding to $A^* = 10^{-2}$ and 10^{-4}. Unless otherwise stated, the results presented below are for conductive surfaces with $D = 2.3$, $G^* = 10^{-7}$, $E/Y = 106$, and $\nu_1 = 0.3$, insulating film with $t = 10$ Å, $K = 6$, and $\varphi_0 = 2$ eV, and applied current $I = 5$ A.

Figure 2 shows the effect of fractal parameters and mechanical properties on the variation of the contact resistance R^* with contact load P^*. For given fractal parameters (i.e., fixed topography) and mechanical properties, the ECR decreases with increasing contact load due to the corresponding increase of the real contact area and the inverse dependence of the ECR on the real contact area [Eq. (22)]. Although for homogenous conductive surfaces the ECR decreases by about two orders of magnitude with the increase of the contact load,[19] for conductive surfaces separated by an insulating thin film the ECR decreases by less than an order of magnitude over the same load range. This is due to the inherent non-Ohmic behavior in the presence of an insulating thin film, where the tunnel resistance of each microcontact increases with decreasing voltage drop across the microcontact.[27] Increasing the contact load results in a lower ECR, which for a fixed current flow *I*, yields a lower

voltage drop. This, in turn, increases the microcontact tunnel resistances, thus compensating the decrease of the total ECR. This phenomenon is observed in the following figures showing the ECR as a function of contact load and, hereafter, will be referred to as the voltage compensation mechanism. The fact that for a given contact load the ECR increases with the fractal roughness G^* [Fig. 2(a)] is attributed to the smaller real contact area obtained with higher G^* values (rougher surfaces). As discussed for isotropic conductive surfaces,[19] Fig. 2(a) can be used to determine G^* from simple measurements of R^*, provided all other parameters are known. Also, the ratio $\varphi_0^{1/2}/t$ can be determined from Fig. 2(a), Eq. (21), the given load, and the measured ECR. The value of P^* determined from the measured ECR can be used to evaluate the adhesion force and interfacial adhesion energy following the method for homogenous conductive surfaces described elsewhere.[34] The last two approaches can also be carried out by using any of the Figs. 2, 4, and 6 presented below.

Figure 2(b) shows the variation of the ECR with contact load and fractal dimension. For a fixed load, increasing the fractal dimension causes the ECR to decrease. This is because larger D values correspond to smoother (denser) surface topographies producing larger real contact areas,[19] which decreases the ECR. The almost identical ECR results obtained for D = 2.1 and 2.2 are due to the very large critical truncated contact area a_c' [Eq. (4)] obtained with such small values of D, resulting in fully plastic deformation of the majority of the microcontacts. In this case the relation between the ECR and the contact load is independent of the surface topography [Eq. (23)]. Therefore, the performance of electrical contacts operating in the fully plastic deformation regime is insensitive to the surface topography, which may exhibit variations depending on the fabrication process and/or the evolution of wear. As for Fig. 2(a), the results shown in Fig. 2(b) can be used to determine the fractal dimension D from the measured ECR and the applied contact load.

Figure 2(c) shows the effect of the mechanical properties of the contacting surfaces on the variation of the ECR with contact load. For a given dimensionless contact load, increasing *E/Y* decreases the ECR. Since the reduced elastic modulus affects both *E/Y* and P^*, it is difficult to draw a general conclusion about the effect of the mechanical properties on the ECR. However, if the reduced elastic modulus is assumed to remain constant, the results shown in Fig. 2(c) can be used to obtain insight into the effect of the yield strength on the ECR. Because the mean contact pressure decreases with yield strength,[21] a larger contact area is required to support a given contact load, resulting in a lower ECR. Figure 2(c) can also be used to determine the yield strength of the softer material or the reduced elastic modulus (through an iterative procedure[19] necessitated by the dependence of *E/Y* and P^* on *E*) from ECR measurements.

As discussed in Ref. 19 for homogenous conductive surfaces, it is advantageous to obtain the real contact area in terms of the ECR because of the independence of this relation on the surface topography and mechanical properties. This is also the case for conductive surfaces separated by a thin insulating film, as can be deduced from Eq. (22) for the low-voltage regime ($V_i \cong 0$). Figure 3 shows the real contact area as a function of the ECR for the entire range of fractal parameters and mechanical properties used to obtain the results shown in Fig. 2. The results were obtained by cross plotting data of R^* (shown in Fig. 2) and A^* (not shown here for brevity) obtained for the same contact load. It is interesting to note that all the data closely follow the same curve even for the general case of $V_i > 0$. This implies that the surface topography and mechanical properties do not influence the dependence of A^* on R^*. This is of great importance in dynamic systems where surface deformation may change the topography.

According to the approximate analysis (Sec. III), the relation between A^* and R^* [Eq. (22)] is a function of *t*, *K*, and φ_0 and is independent of surface topography, mechanical properties, and

contact load, in accord with the results shown in Fig. 3. However, significant differences exist between the results obtained from Eq. (22) and those shown in Fig. 3 due to the assumption of $V_i \cong 0$ invoked in the approximate analysis. According to this analysis, the relation between A^* and R^* is independent of the current used to obtain the ECR measurements, while the accurate solution depends on the applied current through the voltage drop that affects ΔS and φ_L [Eqs. (13) and (15), respectively]. By curve fitting the numerical results shown in Fig. 3, the following empirical relation was obtained:

$$A^* = 3.21\times10^{-2}\exp\left(-2.91\times10^{-7}R^*\right). \quad \textbf{(25)}$$

The proportionality factor and exponent in Eq. (25) are both functions of *t*, *K*, φ_0, and the voltage drop across the interface *V*, i.e., the current *I* used in the ECR measurements.

Figure 4 shows the effects of the dielectric constant, film thickness, and energy barrier height on the variation of the ECR with contact load. For a fixed contact load, the ECR decreases with *K*, *t*, and φ_0, because R_{ti} decreases with these parameters (Sec. IIC). For a given current, a smaller ECR produces a smaller voltage drop across the interface, where the tunnel resistance is Ohmic and, therefore, independent of the voltage drop. This may explain the pronounced variation of the ECR with contact load in these cases, resembling the behavior of homogenous conductive surfaces possessing Ohmic behavior.[19] The results shown in Fig. 4 can be used to determine the dielectric constant, thickness, and energy barrier height of the insulating film from ECR measurements. However, because the dimensionless ECR is also a function of *t* and φ_0 [Eq. (21)], an iterative procedure is required to determine these parameters. Hence, assuming an initial value of the unknown parameter (*t* or φ_0), the dimensionless ECR can be calculated from the measured ECR using Eq. (21). Then Fig. 4(b) or Fig. 4(c) can be used to determine whether the dimensionless ECR

(based on the ECR measurements) coincides with the curve corresponding to the assumed value of the unknown parameter. This procedure can be repeated until eventually a convergence to a specified tolerance value is obtained.

The dependence of the real contact area on the ECR is shown in Fig. 5 for the ranges of dielectric constant, film thickness, energy barrier height, and contact load used to obtain the results presented in Fig. 4. The results were obtained using the same method with that used to obtain the results shown in Fig. 3. As shown in Fig. 5, the relation of A^* versus R^* depends on the insulating film properties. Equation (25) can be written in the general form

$$A^* = \alpha \exp\left(-\beta R^*\right), \tag{26}$$

where α and β assume positive values that depend on *K*, *t*, φ_0, and the current *I* used in the ECR measurements. The values of α and β can be determined by curve fitting the numerical results obtained for the particular film properties, as shown in Fig. 5. The variation of the ECR with real contact area is more pronounced for smaller values of *K*, *t*, and φ_0, due to the absence of the voltage compensation mechanism in these cases (see discussion of Figs. 2 and 4). Therefore, greater accuracy in the determination of the real contact area based on ECR measurements is expected for surfaces covered by relatively thin insulating films possessing both low dielectric constant and energy barrier. As for Fig. 3, the results shown in Fig. 5 are independent of mechanical properties, fractal parameters, and contact load.

Figure 6 shows the effect of the current used in the ECR measurements on the variation of the ECR with contact load. For a fixed contact load, the ECR decreases with increasing current because the tunnel resistance of a microcontact decreases with increasing voltage drop, as discussed in Sec. IIC. This implies that different applied currents may bias the ECR measurements due to the voltage compensation mechanism. Another consequence of this effect could be the inaccurate

estimation of the contact load. The results corresponding to $I \cong 0$ (also shown in Fig. 7) were obtained from Eq. (11). For current equal to 0.1 A, the results obtained by using the voltage-dependent tunnel resistance relations [Eqs. (12) – (15)] are in good agreement with the approximate results corresponding to $I \cong 0$. Relatively small differences occur at very light loads where the ECR assumes high values. In these light load cases, the high voltage drop invalidates the assumption $V_i \cong 0$, even though the current is very low ($I = 0.1$ A). The results for $I \cong 0$ and 0.1 A were also found to be in good agreement with the approximate solution for fully plastic contacts [Eq. (23)], indicating the dominance of fully plastic microcontacts in lightly loaded contact interfaces. With such small currents, the ECR decreases by about two orders of magnitude due to the Ohmic behavior of the tunnel resistance [Eq. (11)], while for higher currents the decrease of the ECR is significantly less (for the same load range) due to the inherent dependence of the ECR on the voltage and the associated compensation mechanism. The results shown in Figs. 4 and 6 suggest that greater accuracy in the determination of the contact load from ECR measurements can be obtained for thin insulating films possessing both low dielectric constant and energy barrier and by applying a low current.

The dependence of the real contact area on the ECR is shown in Fig. 7 for the entire range of electric current used to obtain the results presented in Fig. 6. The results were obtained with the same method used to obtain results shown in Fig. 3. It is noted that the relation between A^* and R^* depends on the current used in the ECR measurements and follows Eq. (26). For current equal to or less than 0.1 A, the results for the voltage-dependent tunnel resistance [Eqs. (12) – (15)] are in good agreement with the approximate results for the voltage-independent tunnel resistance, i.e., $I \cong 0$ [Eq. (11)], except for high ECR values, in agreement with Fig. 6. The results corresponding to $I \cong 0$ (and $I = 0.1$ A for low ECR values) are also in good agreement with the approximate

solution for fully plastic contacts [Eq. (22)] (not shown here for clarity), confirming the dominance of fully plastic microcontacts in lightly loaded contacts. Figure 7 shows that it is advantageous to determine the real contact area from ECR measurements using low currents due to the more pronounced variation of the ECR with real contact area at lower currents, a consequence of the Ohmic behavior of the ECR at low voltages.

VI. CONCLUSIONS

An ECR theory was introduced for conductive and rough (fractal) surfaces separated by a thin insulating film. Results illustrate the importance of an intervening film consisting of an insulating material, contact load, mechanical properties, surface topography, and current intensity in electrical contacts. The analysis accounts for current flow between the surfaces by electron tunneling through a rectangular energy barrier including image forces. Based on the presented results and discussion, the following main conclusions can be drawn.

(1) The constriction resistance plays a secondary role compared to the tunnel resistance and, therefore, the ECR is dominated by the tunnel effect.

(2) The ECR decreases with increasing contact load, fractal dimension D, and current flow, and decreasing fractal roughness G, film thickness, dielectric constant, and energy barrier height.

(3) The variation of the ECR with contact load (or real contact area) is less pronounced than that observed in the absence of the insulating layer due to the intrinsic voltage dependence of the tunnel resistance (non-Ohmic behavior). For the same reason, this variation becomes less pronounced with the increase of the applied current.

(4) For contacting surfaces with small D values (i.e., $D \leq 2.2$) the majority of the microcontacts are in the fully plastic deformation regime and the ECR is independent of surface topography parameters.

(5) For low currents (i.e., $I \leq 0.1$ A), the numerical solutions for the ECR versus contact load and the real contact area versus ECR are in good agreement with closed-form analytical solutions obtained under the assumption of Ohmic contacts and fully plastic deformation of the microcontacts.

(6) The relation between the real contact area and the ECR depends on the current, insulating film thickness, dielectric constant, and energy barrier height and is independent of the contact load and the surface topography and mechanical properties of the contacting surfaces.

ACKNOWLEDGMENTS

This research was supported by the National Institute of Standards and Technology under Grant No. 60NANB1D0078, and the Computer Mechanics Laboratory at UC-Berkeley. The financial support provided to one of the authors (L. K.) by a Fulbright Fellowship and a New-England (Technion) award is also gratefully acknowledged.

REFERENCES

[1] C. G. Karagiannopoulos, P. D. Bourkas, C. T. Dervos, and C. A. Kagarakis, IEEE Trans. Compon. Hybr. Manuf. Technol. **14**, 137 (1991).

[2] M. Antler, IEICE Trans. Electronics **E82-C**, 3 (1999).

[3] K. Sawa and M. Hasegawa, IEICE Trans. Electronics **E83-C**, 1363 (2000).

[4] E. J. J. Kruglick and K. S. J. Pister, J. Microelectromech. Syst. **8**, 264 (1999).

[5] S. Majumder, N. E. McGruer, G. G. Adams, P. M. Zavracky, R. H., Morrison, and J. Krim, Sensors and Actuators A **93**, 19 (2001).

[6] K. Karasawa, Z.-K. Chen, and K. Sawa, Electron. Commun. Jpn. Pt. II-Electron. **80**, 33 (1997).

[7] T. Tamai, A. Sato, and S. Ito, IEEE Trans. Compon. Packag. Technol. **23**, 234 (2000).

[8] A. Mikrajuddin, F. G. Shi, S. Chungpaiboonpatana, K. Okuyama, C. Davidson, and J. M. Adams, Mater. Sci. Semicond. Process. **2**, 309 (1999).

[9] L. Li and J. E. Morris, IEEE Trans. Compon. Packag. Manuf. Technol. A **20**, 3 (1997).

[10] M. Sun, Microelectron. J. **32**, 197 (2001).

[11] E. Crinon and J. T. Evans, Mater. Sci. Eng. A **242**, 121 (1998).

[12] H. H. Law, C. A. Holden, J. Sapjeta, G. R. Crane, and S. Nakahara, IEEE Trans. Compon. Hybr. Manuf. Technol. **14**, 585 (1991).

[13] W. A. Meulenberg, S. Uhlenbruck, E. Wessel, H. P. Buchkremer, D. Stöver, J. Mater. Sci. **38**, 507 (2003).

[14] H. Prashad, J. Tribol. **124**, 468 (2002).

[15] C. V. G. Reddy and S. V. Manorama, J. Electrochem. Soc. **147**, 390 (2000).

[16] J. G. Simmons, Trans. Metall. Soc. AIME. **233**, 485 (1965).

[17] K. Komvopoulos, V. Chiaro, B. Pakter, E. S. Yamaguchi, and P. R. Ryason, Tribol. Trans. **45**, 568 (2002).

[18] R. Holm, *Electrical Contacts*, 4th ed. (Springer, New York, NY, 1967).

[19] L. Kogut and K. Komvopoulos, J. Appl. Phys. **94**, 3153 (2003).

[20] W. Yan and K. Komvopoulos, J. Appl. Phys. **84**, 3617 (1998).

[21] K. Komvopoulos and N. Ye, J. Tribol. **123**, 632 (2001).

[22] A. Mikrajuddin, F. G. Shi, H. K. Kim, and K. Okuyama, Mater. Sci. Semicond. Process. **2**, 321 (1999).

[23] H. C. Angus, Br. J. Appl. Phys. **13**, 58 (1962).

[24] M. D. Bryant and M. Jin, IEEE Trans. Compon. Hybr. Manuf. Technol. **14**, 79 (1991).

[25] J. C. Fisher and I. Giaever, J. Appl. Phys. **32**, 172 (1961).

[26] C. G. Karagiannopoulos, C. S. Psomopoulos, and P. D. Bourkas, Modeling Simul. Mater. Sci. Eng. **9**, 181 (2001).

[27] J. G. Simmons, J. Appl. Phys. **34**, 1793 (1963).

[28] J. A. Greenwood and J. B. P. Williamson, Proc. R. Soc. (London), Ser. A **295**, 300 (1966).

[29] A. Majumdar and C. L. Tien, Wear **136**, 313 (1990).

[30] B. B. Mandelbrot, *The Fractal Geometry of Nature* (Freeman, New York, NY, 1983).

[31] A. Majumdar and C. L. Tien, J. Heat Trans. **113**, 516 (1991).

[32] J. A. Greenwood, Proc. R. Soc. (London), Ser. A **393**, 133 (1984).

[33] D. Tabor, *The Hardness of Metals* (Clarendon, Oxford, UK, 1951).

[34] L. Kogut and K. Komvopoulos, J. Appl. Phys. **94**, (2003) in press.

[35] Y. V. Sharvin, Sov. Phys. JETP **21**, 655 (1965).

[36] J. R. Barber and M. Ciavarella, Int. J. Solids Struct. **37**, 29 (2000).

List of Figures

FIG. 7. Dimensionless contact area A^* versus dimensionless electrical contact resistance R^* for contacting rough surfaces with different mechanical properties and fractal parameters, and various values of applied current I (K = 6, t = 10 Å, and φ_0 = 2 eV).

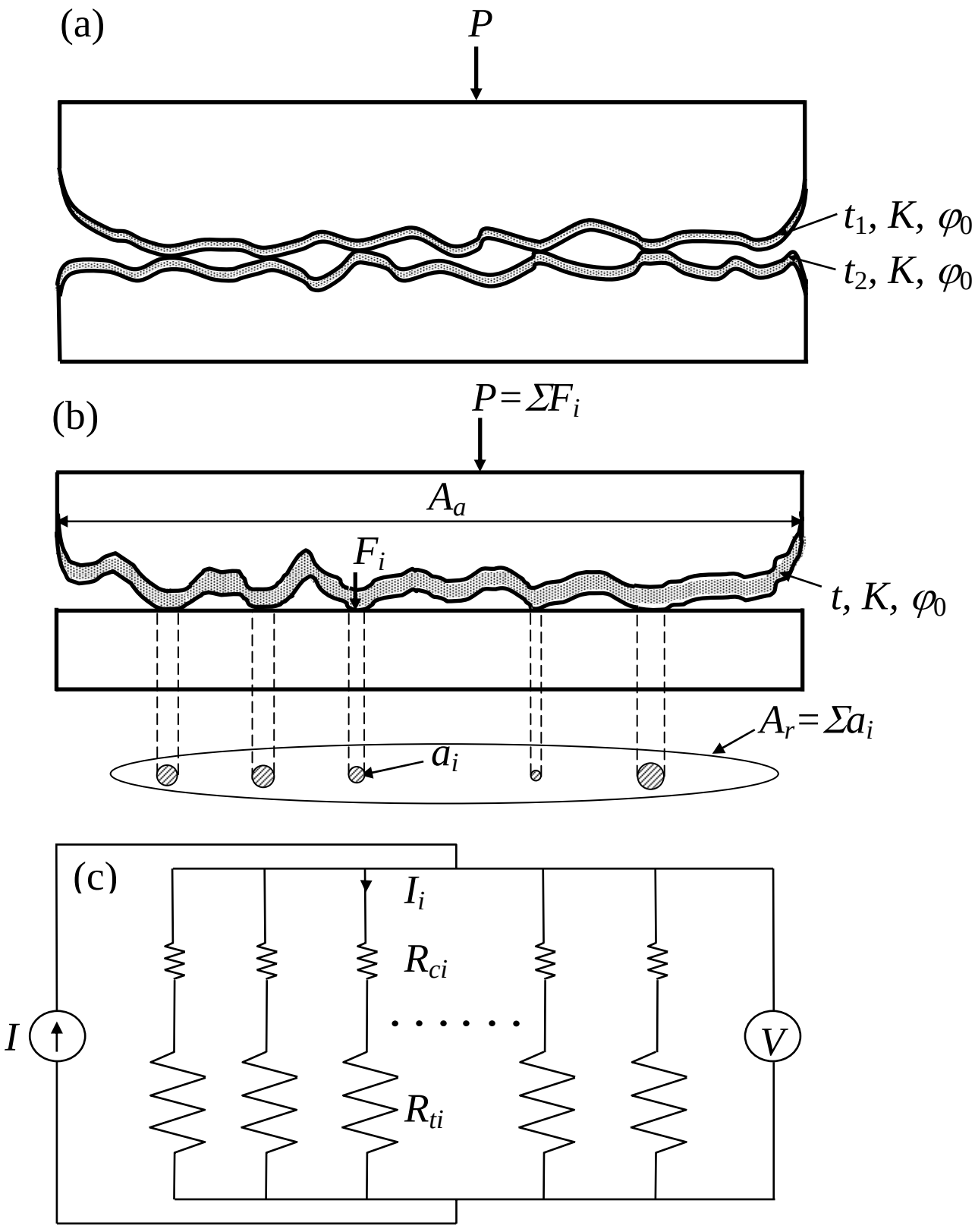

FIG. 1.

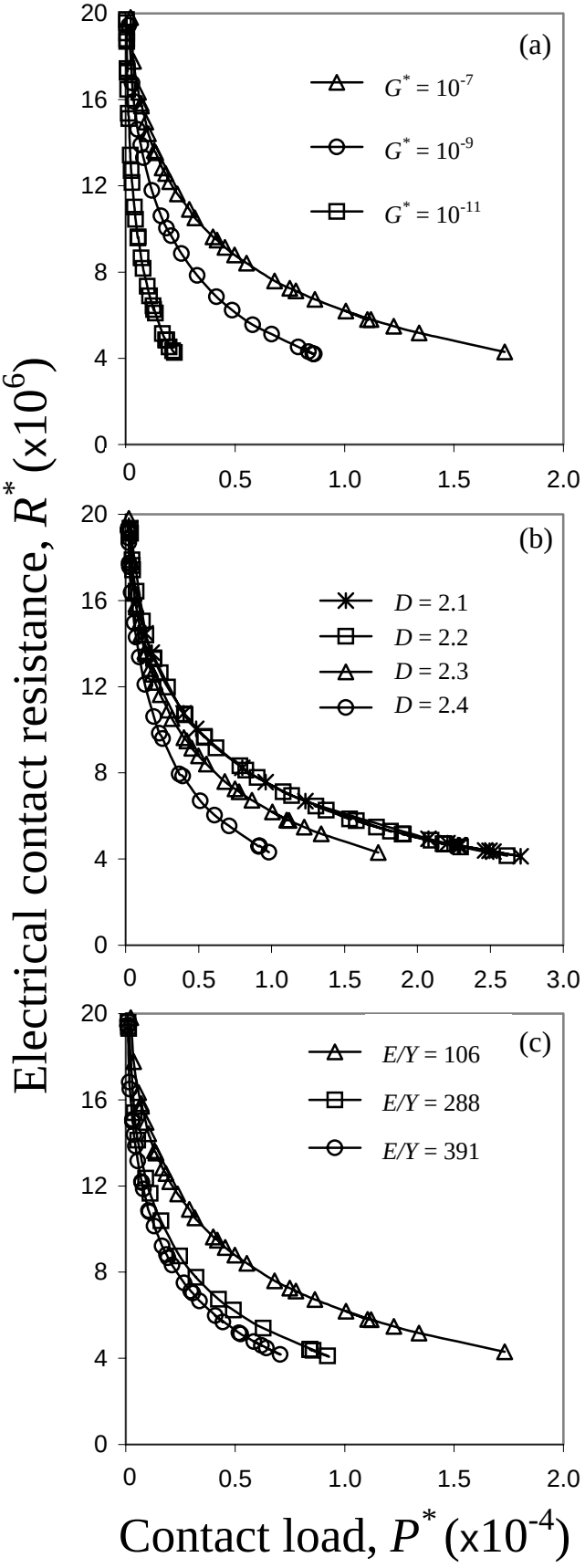
(a)
$G^* = 10^{-7}$
$G^* = 10^{-9}$
$G^* = 10^{-11}$
(b)
D = 2.1
D = 2.2
D = 2.3
D = 2.4
(c)
E/Y = 106
E/Y = 288
E/Y = 391
Electrical contact resistance, R^* (x10^6)
Contact load, P^* (x10^{-4})

FIG. 2.

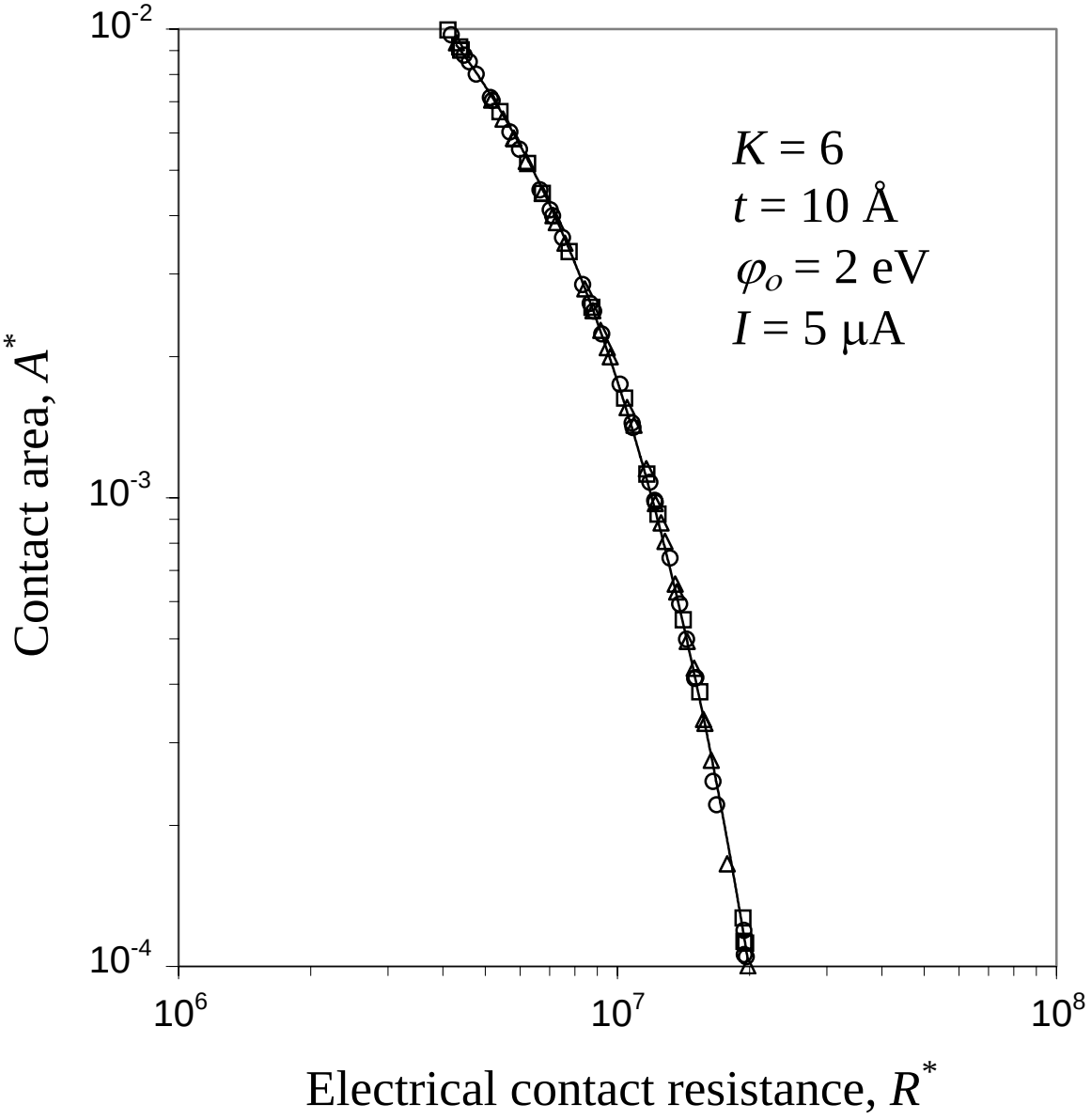
10^{-2}
10^{-3}
10^{-4}
10^{6}
10^{7}
10^{8}
Contact area, A^*
Electrical contact resistance, R^*
$K = 6$
$t = 10$ Å
$\varphi_o = 2$ eV
$I = 5$ μA

FIG. 3.

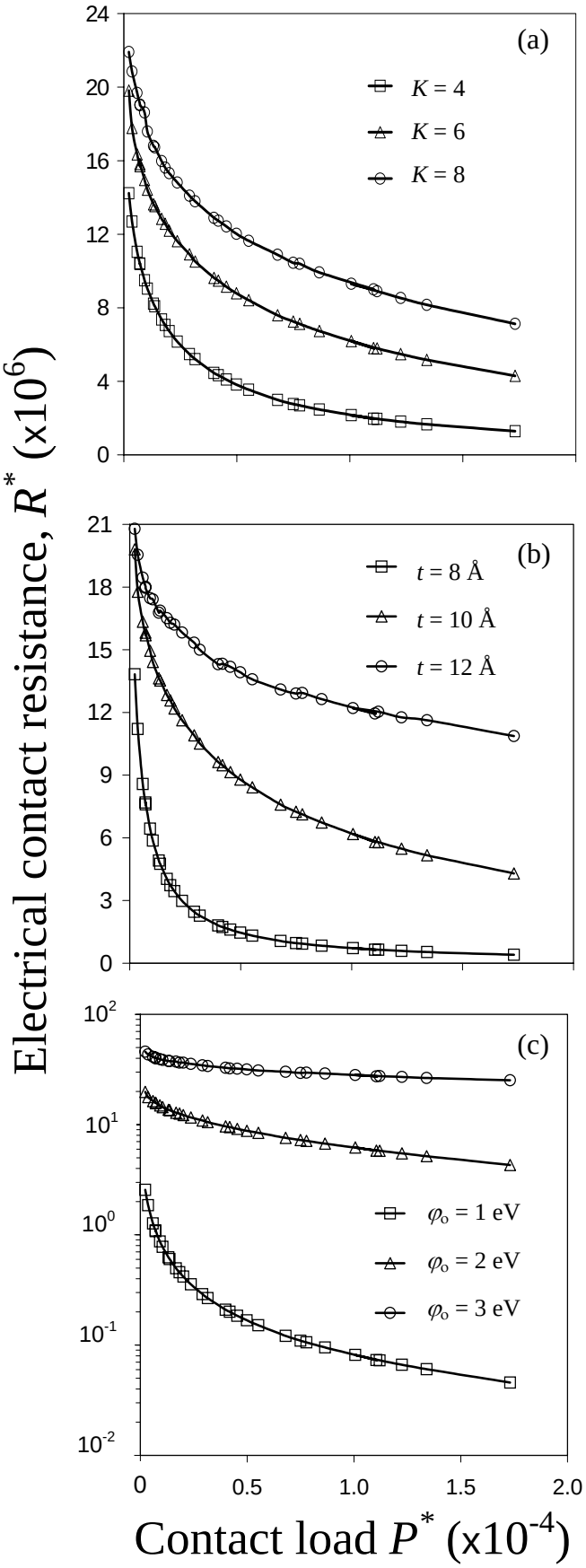
(a)
K = 4
K = 6
K = 8
(b)
t = 8 Å
t = 10 Å
t = 12 Å
(c)
φo = 1 eV
φo = 2 eV
φo = 3 eV
Electrical contact resistance, R* (x10^6)
Contact load P* (x10^-4)

FIG. 4.

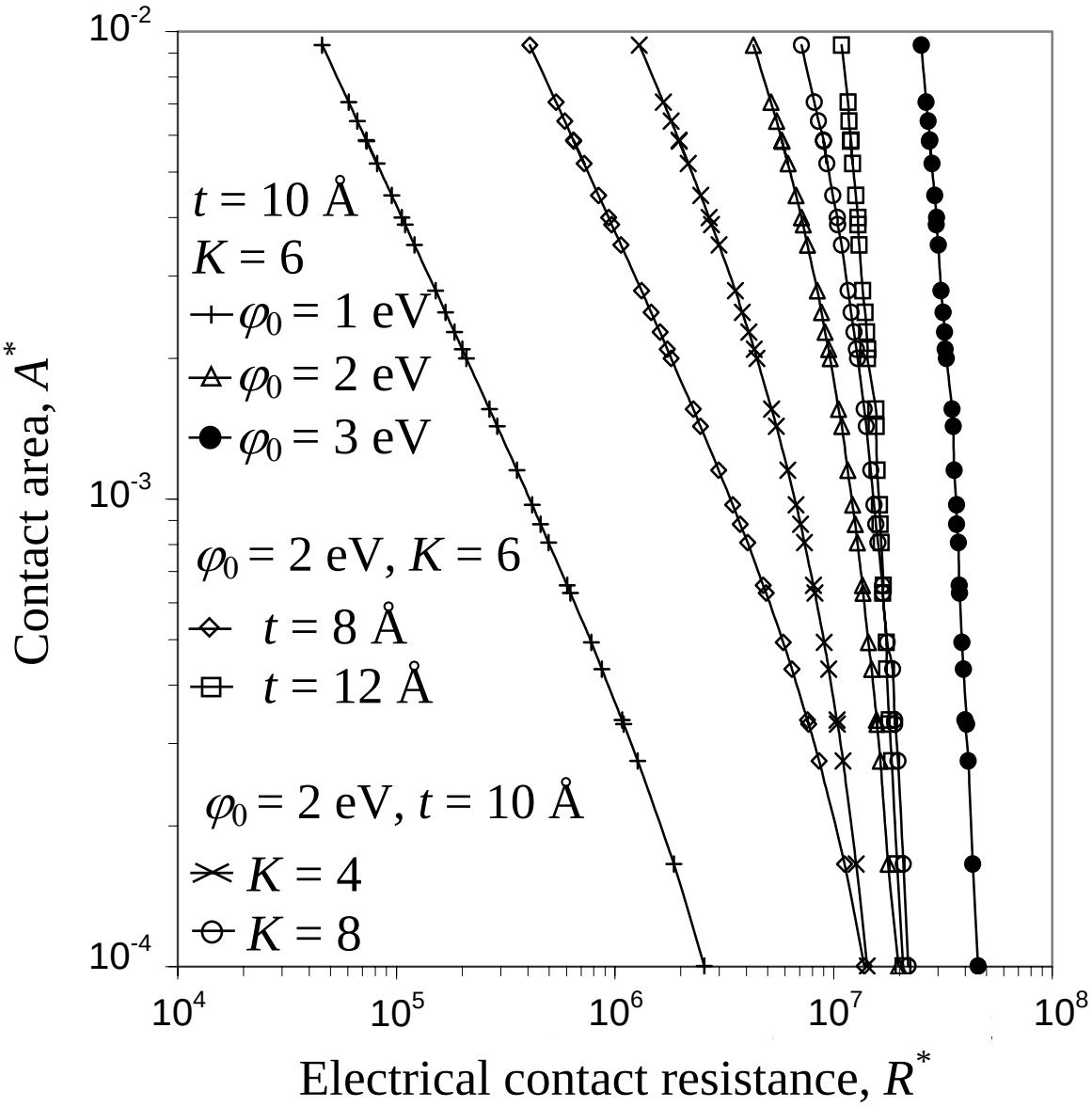
Contact area, A^*
Electrical contact resistance, R^*
10^{-2}
10^{-3}
10^{-4}
10^4
10^5
10^6
10^7
10^8
t = 10 Å
K = 6
φ_0 = 1 eV
φ_0 = 2 eV
φ_0 = 3 eV
φ_0 = 2 eV, K = 6
t = 8 Å
t = 12 Å
φ_0 = 2 eV, t = 10 Å
K = 4
K = 8

FIG. 5.

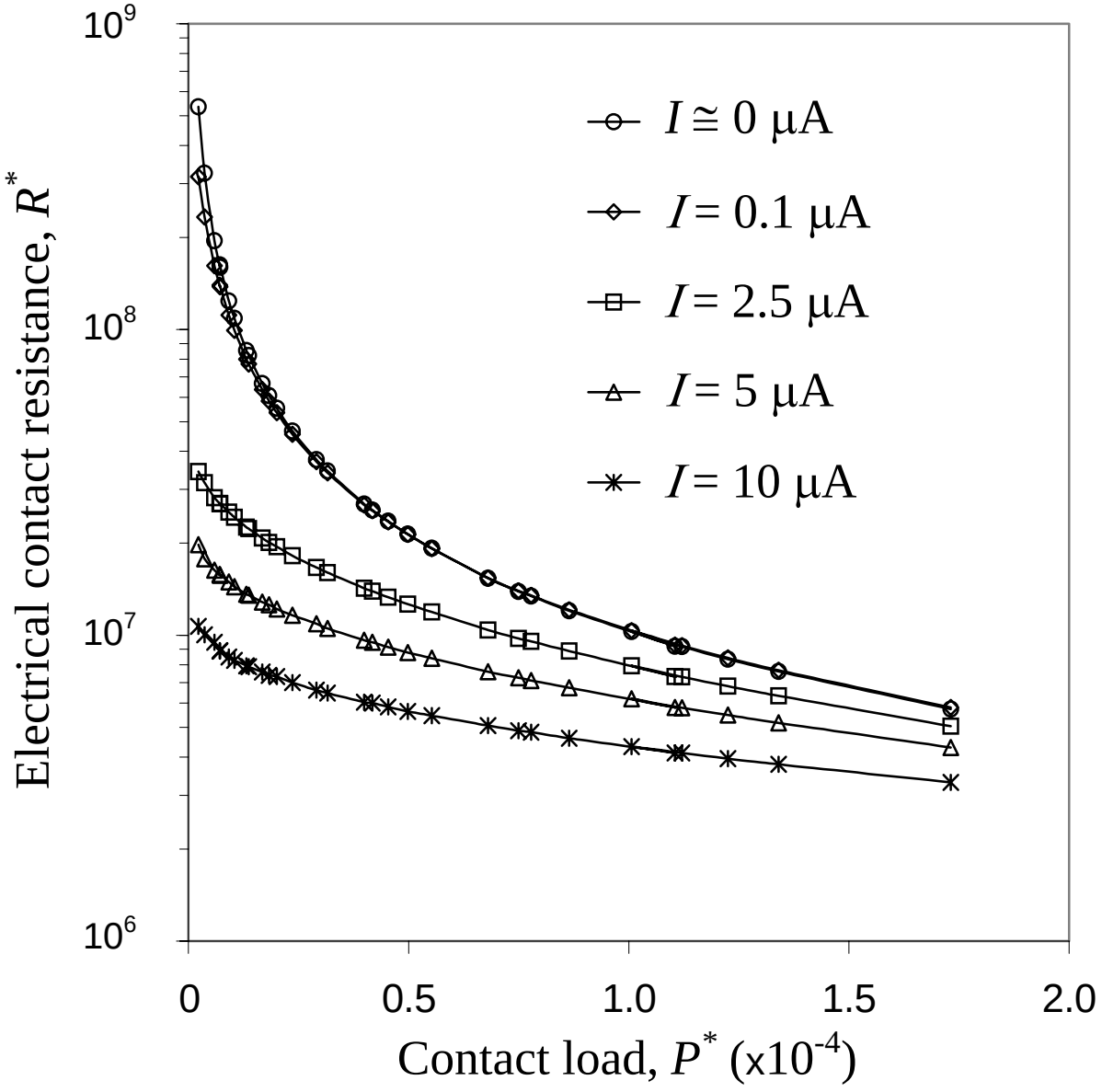
10^9
10^8
10^7
10^6
Electrical contact resistance, R^*
$I \cong 0$ μA
$I = 0.1$ μA
$I = 2.5$ μA
$I = 5$ μA
$I = 10$ μA
0
0.5
1.0
1.5
2.0
Contact load, P^* (x10^{-4})

FIG. 6.

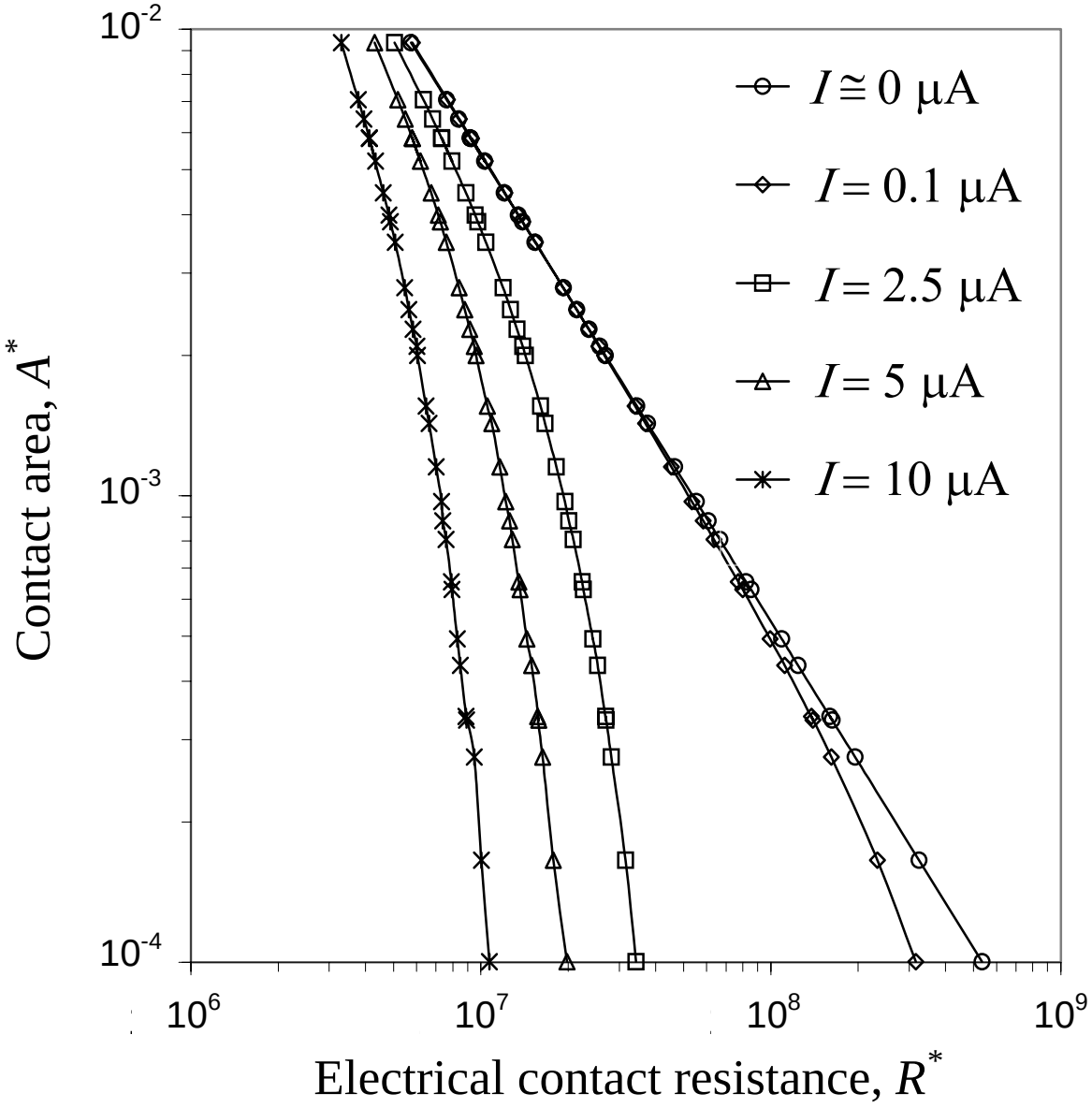
10^{-2}
10^{-3}
10^{-4}
Contact area, A^*
10^6
10^7
10^8
10^9
Electrical contact resistance, R^*
$I \cong 0$ μA
$I = 0.1$ μA
$I = 2.5$ μA
$I = 5$ μA
$I = 10$ μA

FIG. 7.